THE JOURNAL OF PHYSICAL CHEMISTRY C

pubs.acs.org/JPCC Article

Dynamics of RS-(Au-SR)$_x$ Staple Motifs on Metal Surfaces: From Nanoclusters to 2D Surfaces

Pilar Carro, Evangelina Pensa,* Tim Albrecht, and Roberto C. Salvarezza

Cite This: J. Phys. Chem. C 2020, 124, 5452−5459 Read Online

ACCESS | Metrics & More | Article Recommendations | Supporting Information

ABSTRACT: Limited stability of metal nanoparticles hinders their long-term uses and applications. For metal nanoclusters, this is even more critical, as physicochemical properties rely on the structure of only a few hundred atoms. Here, we study the irreversible change that $Au_{25}(SR)_{18}$ suffers upon interaction with 2D metal surfaces. Experimental and density functional theory results allow us to identify the triggering factors of the decomposition process. Our thermodynamic-based approach can be extended to other metal nanocluster/substrates, turning it into a useful tool for predicting the nanoscale stability of these systems.

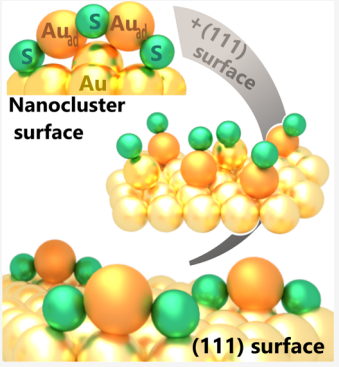

1. INTRODUCTION

Thiolated gold nanoclusters (AuNCs) are made up of a precise number of Au atoms and ligands as a capping layer around the metallic Au cores. This ligand shell consists of staple motifs, whose structure can be represented as polymeric species RS-(Au-SR)$_x$, where RS is the thiyl radical.[1,2] The stoichiometry of the moiety forming the shell varies with the size of the AuNCs.[1] For example, while RS-Au-SR is found in $Au_{144}(SR)_{60}$,[3−5] RS-Au-(SR)-Au-SR features in $Au_{25}(SR)_{18}$.[6−8] Depending on the number of gold atoms in the chain, these complexes are subsequently referred to as monomeric or dimeric staples, respectively.

The staple motifs have been also found in thiolated-self-assembled monolayers (SAMs) on Au(111) surfaces. For short alkanethiolates and some aromatic thiols, experimental and theoretical studies have shown that RS-Au-SR moieties are present on this substrate forming well-ordered lattices.[9−13] The resulting interface is formed upon thiol adsorption as the thiolated molecules extract Au adatoms from the surface leaving Au vacancies, which nucleate into the Au vacancy islands observed experimentally.

We have recently shown that $Au_{25}(SR)_{18}$, as well as $Au_{144}(SR)_{60}$, disintegrate upon interaction with bare Au(111) surfaces, leading to Au islands and thiol-based adsorbates.[14] This effect, similarly observed by other groups,[15,16] also takes place on oxide substrates[17] and appears to be less prominent on Pt(111).[18] Interestingly, the formation of the adsorbed layer may be expected to differ from the one obtained by traditional methods, namely, by incubation in thiol solutions or by vapor deposition. This is because the staple motif has already been formed and its formation energy therefore does not enter in the energy balance of the adsorption process. This raises interesting questions about the mechanism and dynamics of the decomposition process, whether the resulting structure of the adlayer is indeed different and ultimately whether such an approach might be used to control the structure, defect density, and other properties of the interface.

The above questions are important not only for the dynamics of thiolated SAM interfaces on Au(111) but also for doping the AuNCs with a foreign metal.[19−23] Recently, it has been shown that AuNCs can incorporate silver atoms by a cluster−surface metal exchange reaction, where partial AuNC degradation acts as a vehicle for the metal exchange.[19] Thus, the dynamics of the capping layer could influence the incorporation of new metals.[24] Also, controlled decomposition of metallic clusters on foreign substrates opens a new way to prepare highly dispersed catalytic active surfaces with two or three dimensional architectures.[25]

In the present work, we critically discuss the interfacial structure of the thiolated monolayer obtained after $Au_{25}(SR)_{18}$ NCs decompose on Au(111), being RS: *n*-hexanethiol thiyl radical. Scanning tunneling microscopy (STM) imaging, electrochemistry, and density functional theory (DFT) calculations are employed to determine the surface structures present on Au(111) upon its interaction with AuNCs. Based

Received: December 8, 2019
Revised: February 4, 2020
Published: February 6, 2020

https://dx.doi.org/10.1021/acs.jpcc.9b11369
J. Phys. Chem. C 2020, 124, 5452−5459

on these results, we then assess the factors that trigger the AuNC decomposition.

2. EXPERIMENTAL SECTION

2.1. General. The glassware employed in this work was cleaned by immersing it in boiling aqueous 20% HNO_3 solution for ∼30 min. After this, the material was rinsed with ultrapure water and dried in an oven at 80 °C. For the AuNC synthesis, an extra cleaning step with the *aqua regia* solution was carried out in order to remove any metal traces.

All reagents and solvents were purchased from Sigma-Aldrich and were used as received (purity as stated in the text). For aqueous solutions, ultrapure water (H_2O, 18.2 MΩ·cm, Purite Select Fusion 160, UK) was employed.

Two Au(111) substrates were employed. For STM measurements, we used Au(111) single crystal disks (99.999% purity, polished with roughness <0.01 μm, and orientation accuracy <0.1°, MaTecK GmbH, Germany). For electrochemical experiments, we employed preferentially oriented Au(111) substrates (Arrandee, Germany). Prior to use, the two substrates were cleaned as follows. The Au(111) Arrandee substrates were rinsed with a mix of EtOH and H_2O (50% v/v) and then dried with N_2 and finally H_2 flame-annealed for ca. 2 min. The Au(111) single crystal discs were cleaned by electropolishing and H_2-flame annealing. First, a layer of gold oxide was generated by electro-oxidation in chloride-free 0.1 M H_2SO_4 at 5.5 V with a Pt counter electrode. Then, the oxide layer was dissolved by dipping in 1 M HCl. This protocol produced well-defined terraces but also step bunching. To reduce the number of steps, the substrate was annealed in a furnace at 850 °C for 36 h (NaberTherm LE 4/11/R6, Germany). Finally, the substrates were H_2 flame-annealed for ca. 1 min prior to use.

Immersion of Au substrates in AuNC DCM dispersion was performed in the dark at room temperature for the lapse of time indicated in Figure 1e. Along the immersion, the vials were covered with an alumina foil to prevent oxidation of the analytes via ambient light.

2.2. AuNCs Synthesis and Characterization. AuNCs were synthetized and characterized as previously described in ref 14. The hexanethiolate-capped AuNCs were synthetized as previously reported.[14,26] $HAuCl_4·3H_2O$ (400 mg) and 625 mg of tetraoctylammonium bromide (ToABr, 98%, Sigma-Aldrich) were dissolved in 28 mL of tetrahydrofuran (THF, ≥99.9%, Sigma-Aldrich) and stirred for 15 min. Then, 0.72 mL of 1-hexanethiol (95%, Sigma-Aldrich) was added at room temperature and stirred until the solution was completely colorless (≥12 h). Subsequently, 9.6 mL of a fresh $NaBH_4$ solution (1 M, ≥98.0%, Sigma-Aldrich) were rapidly added to the THF mix, and the reaction mixture was stirred for ∼48 h. The product solution was then gravity-filtered to remove any insoluble materials, and the THF was removed (rotary evaporator, room temperature). The product was dissolved in 20 mL of toluene (≥99.9%, Sigma-Aldrich), and the solution was transferred to a separation funnel and extracted 10 times using 40 mL of ultrapure water. The toluene layer was subsequently removed, and the resulting product was filtered and washed thoroughly with MeOH to remove any traces of excess thiol and ToABr. Afterward, the product was collected by dissolving in dichloromethane (DCM), and finally, the DCM was evaporated by drying in a stream of nitrogen; the resulting dried AuNCs were kept at 4 °C in the dark.

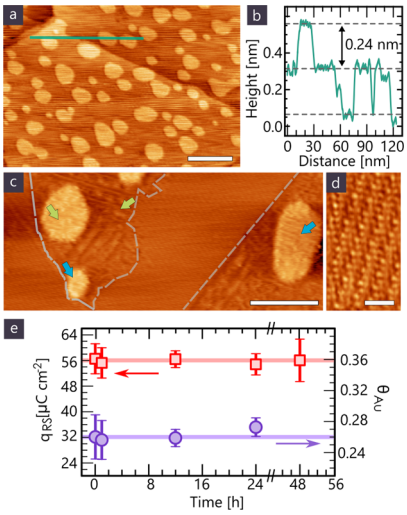

Figure 1. In air STM images and related data showing the spontaneous disintegration of $Au_{25}(SR)_{18}$ NCs on the Au(111) surface. (a) Substrate surface is decorated with Au islands (bright spots). (b) Height profile along green line in (a) showing that the islands are monoatomic in height. (c) RS species in two different domains: the one inside the dotted white line corresponds to a $c(4 \times 2)$ lattice while the rest to RS species randomly distributed. Note that the latter is also on the Au island surface as highlighted by light-blue arrows. The green arrows indicate small agglomerates. (d) High-resolution image of $c(4 \times 2)$ lattice. (e) Time evolution of Au islands coverage (θ_{Au}, purple) and reductive desorption charge of RS adsorbed on the samples (q_{RS}, red). Solid lines indicate the average values. Scale bar in STM images corresponds to 50 (a), 20 (c), and 2 nm (d).

The quality of purification, in terms of unbound thiolated species, was monitored by cyclic voltammetry and STM as follows. The AuNCs were dispersed in MeOH by vigorous shaking. After centrifugation (20 min, 13,400 rpm), the supernatant was collected. Then, Au(111) substrates were immersed for 24 h in the supernatant, rinsed with MeOH, and dried with N_2. Finally, the samples were studied by either cyclic voltammetry or STM. Voltammograms and STM images did not show characteristic features ascribed to thiolates on Au[14] indicating that the unbound thiolates were largely removed after the purification steps were performed.

The presence of the desired AuNCs was confirmed by multiple techniques, as it was previously shown in ref 14, namely, atomic force microscopy, STM, differential pulse voltammetry, and UV−vis spectroscopy.

2.3. Electrochemistry. Electrochemical experiments were performed with a CHI760C potentiostat (CH Instruments, United States) and a conventional three-electrode glass cell. Pt coil and Au substrates were used as counter and working electrodes (WE), while a saturated calomel electrode served as the reference electrode. Cyclic voltammograms (CVs) were recorded in 0.1 M NaOH (99.99%, Sigma-Aldrich) aqueous electrolyte at room temperature (∼25 °C). The electrolyte was degassed with Ar before the measurements, while an Ar atmosphere was maintained throughout the experiments.

The WE was prepared as follows: the Au(111) Arrandee substrates were cleaned and annealed as described above. Subsequently, the substrate was immersed in 2 μM $Au_{25}(SR)_{18}$ dispersed in DCM for the time stated in Figure 1e, rinsed with DCM, and dried with N_2.

https://dx.doi.org/10.1021/acs.jpcc.9b11369
J. Phys. Chem. C 2020, 124, 5452−5459

2.4. Scanning Tunneling Microscopy. STM measurements were performed using a Keysight 5100 STM (Keysight Technologies, United States). STM tips were prepared by mechanically cutting of a Pt/Ir wire (80:20%, 0.25 mm diameter, Goodfellow, UK). All images were acquired in a constant-current mode using the tunneling conditions listed in Table S1. All images are shown with line-wise flattening to remove tilt in the substrate plane. STM calibration was performed for each experiment by analyzing both the HOPG surface (x−y) and Au steps (z). STM images were analyzed with the WSxM software (Nanotec Electronica S.L., Spain).[27]

Samples were prepared by immersing Au(111) single crystals in 2 μM $Au_{25}(SR)_{18}$ dispersed in DCM for the lapse of time stated in Figure 1e, rinsed with DCM, and dried with N_2. As shown in Figure S1, in all cases, the Au(111) substrate was measured before immersing in the AuNC dispersion to assure that the observed features result only from the AuNC/Au(111) interaction.

2.5. Calculations Based on DFT. Calculations were performed using the projector augmented wave method,[28] as implemented in Vienna Ab initio Simulation Package (VASP).[29−31] The valence electrons were described within a plane-wave basis set and an energy cutoff of 420 eV, the remaining electrons were kept frozen as core states. Electron exchange−correlation was represented by the functional of Perdew, Burke, and Ernzerhof of generalized gradient approximation.[32] The weak van der Waals force were treated by the semi empirical method of Grimme (DFT-D) where the dispersion correction term is added to the conventional Kohn−Sham DFT energy[33] with the parametrization DFT-D3.[34] The energy convergence criterion was 10^{-5} eV for SCF energy. The atomic positions were relaxed until the force on the unconstrained atoms was <0.03 eV $Å^{-1}$. The calculated Au lattice constant is 4.099 Å, which compares reasonably well with the experimental value (4.078 Å).[35] The $Au_{25}(RS)_{18}$ NC consists of an icosahedral Au_{13} kernel which is wrapped by six RS-Au-RS-Au-SR dimeric staples. For all NC structures calculated in this work, $Au_{25}(RS)_{18}$, Au_{25}, and Au_{13}, the same cubic cell has been used of 50 Å × 50 Å × 50 Å where the NC is separated by at least 22 Å of vacuum in all three directions. In these cases, the numerical integration was done only in the Γ point. All atomic positions of both Au metal and adsorbates in the AuNCs were allowed to relax in the optimization. On the other hand, the Au(111)-(1 × 1) substrate was represented by five atomic layers and a vacuum of ∼17 Å that separates two successive slabs in our calculation. Surface relaxation was allowed in the three uppermost Au layers of the slab, while the atomic coordinates of the adsorbed species were allowed as well to relax without further constraints. Adsorbates were placed just on one side of the slab, and all calculations include a dipole correction. Optimal grid of Monkhorst−Pack[36] k-points 5 × 4 × 1 and 3 × 9 × 1 were used for numerical integration in the reciprocal space of the $(3 \times 2\sqrt{3})$ and $(3\sqrt{3} \times \sqrt{3})R30°$ unit cell, respectively. In the case of gas-phase species was employed an orthogonal cell of appropriated size. Spin polarization was considered in all gas-phase species.

The RS and complex binding energies on $Au_{25}(RS)_{18}$ and both $(3\sqrt{3} \times \sqrt{3})R30°$ and $c(4 \times 2)$ unit cells on Au(111) flat surfaces, E_b, are defined as follows

$$(E_b^{RS})_{NC} = \frac{1}{18}(E[Au_{25}(RS)_{18}]_{NC} - E[Au_{25}]_{NC} - 18E[RS]_{gas}) \quad (1)$$

$$(E_b^{complex})_{NC} = \frac{1}{6}(E[Au_{13}(Au_2(RS)_3)_6]_{NC} - E[Au_{13}]_{NC} - 6E[Au_2(RS)_3]_{gas}) \quad (2)$$

$$(E_b^{RS})_{Au(111)} = \frac{1}{nx}(E[Au_m(RS)_n]_{Au(111)} - E[Au_m]_{Au(111)} - nxE[RS]_{gas}) \quad (3)$$

$$(E_b^{complex})_{Au(111)} = \frac{1}{x}(E[Au_m(RS)_n]_{Au(111)} - E[Au_{slab}]_{Au(111)} - xE[Au_m(RS)_n]_{gas}) \quad (4)$$

where the NC/Au(111) subscript stands for the NC/Au(111) surface and the RS/complex superscript refers to the species with respect to which the binding energy is calculated. On the other hand, m/n is the Au/RS number in the dimeric (2/3) or monomeric (1/2) staple and x represents the number of complexes in the unit cell [1 in $(3\sqrt{3} \times \sqrt{3})R30°$ and 2 in $c(4 \times 2)$]. A negative number indicates that adsorption is exothermic with respect to the separate clean surface and the adsorbate in the gas phase. On the other hand, the Gibbs free energy of adsorption of each surface structure (γ) can be approximated through the total energy from DFT calculations and the area (A) by using eqs 1−4

$$\gamma = \frac{n}{A}E_b \quad (5)$$

3. RESULTS AND DISCUSSION

The decomposition of $Au_{25}(SR)_{18}$ on Au(111) was first studied by STM and electrochemistry. Figure 1a−d shows the STM images and related data of Au substrates after immersion in $Au_{25}(SR)_{18}$ dispersions (12 h, 2 μM in DCM). The substrates are characterized by the presence of Au islands (0.24 nm in height, Figure 1a,b), and RS species arrange in two domains, as shown in Figure 1c (features absent on bare Au substrates, see Figure S1). In the first molecular arrangement, RS species appear to be randomly distributed in that no long-range order could be observed (outside the dashed lines). This type of domain is observed on Au islands and their surroundings (see light-blue arrows). The other kind of RS domains, included in the dotted line, corresponds to RS moieties in a $c(4 \times 2)$ lattice, as shown in the high-resolution images in Figure 1d.

However, despite the formation of the $c(4 \times 2)$ lattice, there is no evidence of vacancy islands (pits) and serrated steps (Figure 1a), common features when hexanethiolate SAMs on Au(111) are prepared from either gas or liquid phases. This clearly suggests that the mechanism leading to the formation of the $c(4 \times 2)$ lattice does not involve adatom removal from the Au(111) surface, as these are now provided by the gold clusters.

Figure 1e shows the time evolution of both Au island coverage (θ_{Au}) and the reductive desorption charge of the thiolate (q_{RS}), cf. Figures S2/S3 and related notes. Both parameters reach constant values of $\theta_{Au} = 0.26 \pm 0.02$ and $q_{RS} = 56 \pm 2$ μC cm^{-2} after approximately 30 s, indicating that the

https://dx.doi.org/10.1021/acs.jpcc.9b11369
J. Phys. Chem. C 2020, 124, 5452−5459

disintegration process happens within this timeframe. The thiolate coverage is θ_{RS} = 0.25, corresponding to about 3/4 of the expected maximum thiol surface coverage θ_{RS} = 1/3 for the $c(4\times2)$ lattice,[9] in line with the observation of the disordered domains shown in Figure 1c (where the molecules are not close packed).

Importantly, the invariance in θ_{Au} and q_{RS}, at least in the time scale of our observations, rules out the continuous deposition of AuNCs. In fact, increasing the time only leads to a redistribution of both the RS lattice and the Au islands—mainly by increasing the domain and island size, respectively, see discussion below.

Thus, a global picture of the decomposition process could be described as follows: a fixed number of single AuNCs reaches the Au(111) surface and decomposes leading to Au islands and a thiolated monolayer. The degradation reaction is stopped or becomes very slow when the reactivity of Au substrate is sufficiently low, for example, due to adsorbed RS species. In the following, we explore this hypothesis in more detail from a theoretical perspective.

3.1. Thermodynamic Analysis of the Decomposition Process. First, we focus on the thermodynamic analysis of the AuNC decomposition to understand why the $Au_{25}(SR)_{18}$ clusters decompose into the thiolated-$c(4\times2)$ lattice and Au islands when adsorbed on the Au(111) surface. To this end, DFT is employed, see Experimental Section for details.

Theoretical calculations have been focused to shed light into the following observations. Before AuNC decomposition, RS species are only part of the dimeric staple, while upon interaction with the Au surface, they are part of the monomeric staple. The latter is supported by two independent observations, namely, the existence of the $c(4\times2)$ lattice and the Au island coverage expected after the decomposition process, assuming the presence of one Au atom in the monomeric staple that make up the $c(4\times2)$ lattice. The Au coverage estimated from the θ_{RS} value is 0.22, in good agreement with the one obtained by STM imaging analysis 0.26 (cf. Supporting Information for the complete derivation).

Accordingly, we calculate the RS binding energy (E_b) and the surface free energy (γ) of the dimeric staple on the $Au_{25}(SR)_{18}$ cluster and in a $(3\sqrt{3}\times\sqrt{3})R30^\circ$ lattice on Au(111) surface and the monomeric staple in the $c(4\times2)$ lattice on Au(111) (Figure 2a–c). Table 1 shows the E_b and γ values obtained after optimization of each surface structure. Note that here, we focused on electronic energies at equilibrium and zero temperature, that is, we have neglected vibrational and entropic contributions. Nevertheless, entropic factors are expected to favor the decomposition independently of the mechanism taking place.

First, we note that the E_b on the Au(111) surface is higher in the monomeric than in the dimeric staple. This result is not surprising as in the monomeric complex (RS-Au-SR), each S atom is bonded not only to the central Au adatom but also to Au surface atoms. In the dimeric staple motif, only two of the three S atoms interact with Au surface atoms (Figure 2a/b), while the third RS in the middle of the dimeric complex is not bonded to the Au surface atoms. Moreover, when the binding energy of the dimeric staple is compared for the NC and the (111) surface, the higher value on the surface is due to the more favorable configuration of the alkanethiol chains in the SAM.

However, E_b is only an indication of how strong RS species are bonded to the Au substrate. The thermodynamic stability

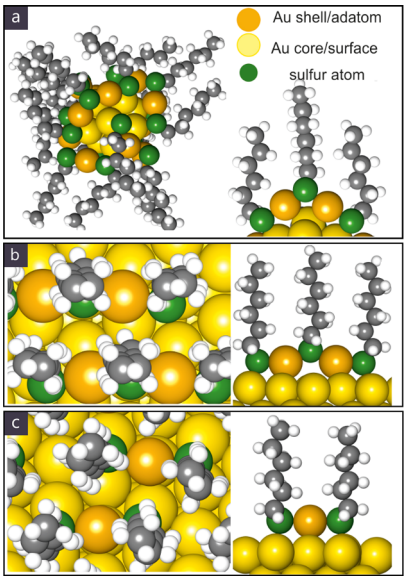

Figure 2. (a) Optimized structures of (a) $Au_{25}(SR)_{18}$ cluster, (b) RS-Au-(RS)-Au-SR on Au(111), and (c) RS-Au-SR on Au(111). Left panel in (a) shows the complete AuNC structure, while panels (b,c) show a top view of the surface structures. Right panels show a side view of the structures. Color code: Au, yellow; Au atoms in RS-Au-(SR)-Au-SR and RS-Au-SR complexes, orange; S atoms, green; C atoms, grey; and H atoms, white.

Table 1. RS Binding Energy (E_b) and Surface Free Energy (γ) for the Different Surface Structures

structure	E_b [eV]	γ [meV Å^{-2}]
$[Au_{25}(SR)_{18}]_{NC}$	−2.96	−166.91
[RS-Au-SR]@Au(111)$_{c(4\times2)}$	−3.47	−158.96
[RS-Au-(RS)-Au-SR]@Au(111)[a]	−3.23	−148.04

[a]Note that for steric reasons RS-Au-(SR)-Au-SR cannot be accommodated in a $c(4\times2)$ lattice. Hence, the staples were arranged in a $(3\sqrt{3}\times\sqrt{3})R30^\circ$ which has the same nominal coverage (θ_{SR} = 1/3).[9]

of the system is given by the free surface energy, γ. As shown in Table 1, the dimeric staple on the AuNC is the most stable, even compared to the monomeric form in the $c(4\times2)$ lattice on Au(111). Interestingly, the stability of this $c(4\times2)$ RS-Au-SR lattice is larger than that estimated when the same thiol lattice is obtained by direct thiol adsorption from gas or solution phases (E_b = −2.95 eV),[37] as in our case, the Au adatoms are provided by the cluster decomposition and no reconstruction energy (E_{rec}) is needed to remove them from the substrate.[38]

Nevertheless, it is evident that the highest stability in terms of γ corresponds to the RS-Au-(SR)-Au-SR complexes on the AuNC because, in spite of their lower E_b, they exhibit a larger adsorbate density on the cluster than on the Au(111) surface (n/A term in eq 5). Thus, it is evident that the thiol stability by itself cannot explain the decomposition process.

Therefore, we analyzed the overall decomposition reaction that, as shown in eq 6, includes the fate of the Au atoms in the cluster and the experimentally observed features—that is, the formation of monoatomic-height Au islands and the presence of the $c(4\times2)$ lattice, presumably formed by RS-Au-SR complexes with the AuNC as the source of Au adatoms.

https://dx.doi.org/10.1021/acs.jpcc.9b11369
J. Phys. Chem. C 2020, 124, 5452−5459

$$[Au_{25}(SR)_{18}]_{NC} + \frac{17}{2}Au(111)_{c(4\times2)} \rightarrow 4[Au_4@Au(111)]_{c(4\times2)} + \frac{9}{2}[RS\text{-}Au\text{-}SR]_2@Au(111)_{c(4\times2)} \quad (6)$$

The energy balance of the above reaction (ΔE) is determined from the respective DFT total electronic energies as

$$\Delta E = \frac{9}{2}E\{[RS\text{-}Au\text{-}SR]_2@Au(111)\}_{c(4\times2)} + 4E[Au_4@Au(111)]_{c(4\times2)} - E[Au_{25}(SR)_{18}]_{NC} - \frac{17}{2}E[Au(111)]_{c(4\times2)} \quad (7)$$

resulting in $\Delta E = -23.2$ eV, suggesting that the decomposition process is indeed energetically favorable.

In order to disentangle the different energetic processes that, besides the RS stability, contribute to the decomposition, we have broken down reaction (6) into four steps following ref 39,

(1) desorption of 18 RS and 25 Au species from the cluster to the gas phase (ΔE_1)

$$Au_{25}SR_{18} \rightarrow 25Au_{gas} + 18RS_{gas} \quad (8)$$

(2) formation of the maximum number of RS-Au-SR species in the gas phase (ΔE_2)

$$18SR_{gas} + 9Au_{gas} \rightarrow 9[RS\text{-}Au\text{-}SR]_{gas} \quad (9)$$

(3) adsorption of the RS-Au-SR moieties in the $c(4 \times 2)$ lattice on the Au(111) surface (ΔE_3)

$$9[RS\text{-}Au\text{-}SR]_{gas} + \frac{9}{2}Au(111)_{c(4\times2)} \rightarrow \frac{9}{2}\{[RS\text{-}Au\text{-}SR]_2@Au(111)]_{c(4\times2)} \quad (10)$$

(4) Au island formation (Au_4) on the Au(111) from Au atoms in the gas phase (ΔE_4)

$$16Au_{gas} + 4Au(111)_{c(4\times2)} \rightarrow 4[Au_4@Au(111)]_{c(4\times2)} \quad (11)$$

Table 2 shows the energetic balance of each step as well as the resulting sum (ΔE_t). ΔE_t agrees with ΔE from the global reaction as established by Hess' law. Importantly, its negative value explains the spontaneous decomposition of the thiol-capped clusters on the Au(111) surface and highlights the key role of the Au atoms (ΔE_4) as the determining factor favoring the spontaneous cluster decomposition.

Table 2. Energetic Values for Reactions 8−11

ΔE_1 [eV]	ΔE_2 [eV]	ΔE_3 [eV]	ΔE_4 [eV]	ΔE_t[a] [eV]
+114.0	−45.4	−40.9	−50.9	−23.2

[a]$\Delta E_t = \Delta E_1+\Delta E_2+\Delta E_3+\Delta E_4$.

Notably, when the energetic balance shown in eq 7 was applied to AuNCs on Ag(111), preliminary DFT calculations suggest that the AuNC decomposition would take place on the Ag(111) surface, in line with the recent experimental results observed on polycrystalline Ag.[19] The latter suggests that the proposed energetic balance could be extrapolated to the other NC-metal surface system, as long as the surface structures in the initial and final states are known.

We have thus shown that the thermodynamic stability of the AuNC depends on a delicate energy balance between the adsorption strength of the ligand−shell to the metal−core and the cohesive energy of the core.[40] This balance is perturbed when the AuNCs are placed in contact with the substrate which induces the transfer of thiol species and Au shell atoms to the (111) metal surface. On the other hand, the entropic factors (not included here) would favor in transferring the thiolates to the Au(111) surface by decomposition of the capping layer into smaller units, as reported recently for organic molecules on Cu(111).[41]

3.2. Toward a Plausible Mechanism for the Au-RS-Au-SR-Au →RS-Au-SR Decomposition. Taking into account the above discussion, as well as previous reports, we will now discuss how thiolated species can be transferred from the AuNC to the clean Au(111) surface.

Figure 1c shows that the regions with ordered $c(4 \times 2)$ lattice are far apart from the islands (see dotted lines) and that the island surfaces and their surroundings exhibit the same type of disorder (light-blue arrows) and include small agglomerates (green arrows). The disorder in thiolated SAMs has been proposed as evidence of mobile species. To test that, in situ STM images with AuNCs in mesitylene were taken. Figure 3a/b shows that thiol molecules rearrange into

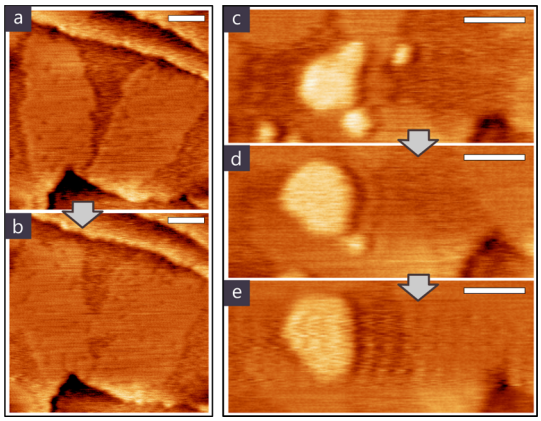

Figure 3. Consecutive STM images showing the temporal dynamics of (a,b) the RS $c(4 \times 2)$ domain and (c−e) Au islands. Images were taken in mesitylene at intervals of 350 s for (a/b), 86 s for (c/d), and 270 s for (d/e). Scale bars correspond to 20 nm (a/b) and 15 nm (c−e).

$c(4 \times 2)$ domains, increasing their boundary sizes (d) with time (t). In fact, if the domain boundaries move by incorporating mobile species, we can estimate the surface diffusion coefficient (D) as $d^2 = 2Dt$, resulting in $D \approx 8 \times 10^{-17}$ cm^2 s^{-1} (cf. Figures 3a/b and S4). This value is closer to the Au atom diffusion coefficient than to that of thiols in dense lattices.[42,43] On the other hand, simultaneously with the thiol species rearranging into $c(4 \times 2)$ domains, the gold islands increase in size at the expense of the smaller ones (Figure 3c−e). This suggests that coalescence and Ostwald ripening take place in order to decrease the surface free energy of the system.

It has been shown that molecular diffusion in alkanethiol SAMs on Au(111) involves mobile RS-Au moieties.[44] These monocoordinated sulfur−metal complexes have been found either along the formation of the SAM or at low SAMs

https://dx.doi.org/10.1021/acs.jpcc.9b11369
J. Phys. Chem. C 2020, 124, 5452−5459

coverage. In the latter case, it has been proposed that RS-Au-SR complexes break apart into RS-Au species on Au(111) at room temperature (RT).[45,46] On the other hand, for carbene SAMs, the carbene−Au complexes displace on Au(111) surfaces by a ballbot-type motion.[47] At RT, the carbene−Au species exhibits practically the same activation barrier for surface diffusion than a plain gold adatom (E_d = 0.1 eV). For thiolated molecules, in contrast, bi- and tri-coordinated sulfur−metal complexes exhibit six times larger activation barriers than the metal adatom.[48] This is reasonable because the mobility of the sulfur−metal complexes such as RS-Au-SR and Au-(SR)-Au-SR should be limited due to the additional S-metal bonds[10,49] and also by the larger binding energy of the entire species on the Au(111) surface (E_b,Table 3).[50]

Table 3. Energetic Values for the RS, Au, and RSAu Complexes on Au(111)

species	E_b [eV]
Au	−2.93
RS	−2.66
Au-SR	−3.09
[RS-Au-SR]	−4.55
RS-Au-(SR)-Au-SR	−5.76

Thus, we propose that RS-Au, RS, and Au adatoms are the predominant species involved in mass transport from the AuNC to the Au(111) surface, according to the following steps

$$AuNC_{sol} \rightarrow AuNC_{Au(111)} \quad (12a)$$

After cluster physisorption on the Au(111) surface (12a), the protective shell and, accordingly, the overall AuNC, becomes unstable by transferring thiolated-gold staples and exposed core gold atoms to the substrate by a curvature-driven process—that is, structures with high-curvature decay into more flat ones by surface diffusion.[51,52] The RS-Au-(SR)-Au-SR moiety disintegrates into mobile RS-Au and RS species according to

$$\text{RS-Au-(SR)-Au-SR} \rightarrow \text{RS-Au-SR} + \text{RS-Au} \quad (12b)$$

$$\text{RS-Au-SR} \rightarrow \text{RS-Au} + \text{RS} \quad (12c)$$

These steps are sketched in Figure 4. Particularly, step 12b has been also proposed in the formation of AuNC dimers[53]

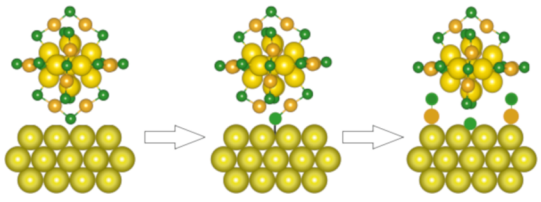

Figure 4. Scheme of the proposed generation of RS-Au and RS species. Color code: Au, yellow; Au atoms in the dimeric complex, orange; and S: green. For clarity, C and H atoms are not included.

and AgNCs doped with Au atoms.[20] Following step 12c, the thiyl radical can react with excess Au adatoms coming from the cluster and yielding RS-Au

$$\text{RS} + \text{Au} \rightarrow \text{RS-Au} \quad (12d)$$

However, as the surface density of mobile RS-Au and RS species increases, they rearrange into the RS-Au-SR moieties locked in the position by neighboring species to form the more stable $c(4 \times 2)$ RS-Au-SR surface structure (Table 1). Thus, we can write

$$2\text{RS-Au} \rightarrow \text{(RS-Au-SR)} + Au_{ad} \quad (12e)$$

Finally, the excess of gold atoms from the AuNC core (12a) and those gold adatoms (Au_{ad}) from decomposition of RS-Au-(SR)-Au-SR (12e) rearrange into Au islands (Au_{island}) species[54] (12f and 12g), as shown STM images in Figure 3c−e.

$$nAu_{NC} \rightarrow nAu_{island} \quad (12f)$$

$$nAu_{island} + Au_{ad} \rightarrow (Au_{n+1})_{island} \quad (12g)$$

4. CONCLUSIONS

In summary, by a combined experimental and theoretical study, we found that AuNC decomposition on the Au(111) surface leads to the complete disintegration of the AuNCs. This process involves the disassembly of the capping layer from RS-Au(SR)-Au-SR into RS-Au-SR units. We have proposed a complete mechanism for such a decomposition that involves multiple surface-step reactions, reflecting the strong structural dynamics of SR-$(Au\text{-}SR)_x$ complexes.

From thermodynamic considerations, we found that the decomposition process is triggered by two energetic factors: the stability of thiolated species on the AuNC versus on the metal and the stability of Au atoms (produced by AuNC core decomposition) on the metal surface. We also show that the above DFT thermodynamic approach predicts the already observed decomposition on Ag(111) surfaces. Thus, we believe that the thermodynamic approach followed in this work can be extrapolated to other metal NCs/substrates systems, as long as the surface structures in the initial and final states are known. Thus, further studies on metal surfaces with well-defined surface crystal structure are needed, in order to get deeper insight into the underlying processes, including exchange reactions.

With regard to the formation of the alkanethiol self-assembly monolayer on Au(111), we found that the AuNC decomposition resulting SAMs lack in one of their typical surface defects, the Au vacancy islands. This fact confirms that the Au vacancy islands formed upon adsorption of thiols on Au(111) are in fact related to the "extraction of Au adatoms" to form RS-Au-SR complexes. Importantly, this new method to obtain alkanethiol SAMs (i.e., via AuNC decomposition) could help to improve their quality and stability, a long-time goal in technological applications of these layers.

■ ASSOCIATED CONTENT

Supporting Information

The Supporting Information is available free of charge at https://pubs.acs.org/doi/10.1021/acs.jpcc.9b11369.

Additional STM images and electrochemical data (PDF)

■ AUTHOR INFORMATION

Corresponding Author

Evangelina Pensa − *Department of Chemistry, Imperial College London, London SW7 2AZ, U.K.;* orcid.org/0000-0003-1090-0830; Email: e.pensa@tum.de

https://dx.doi.org/10.1021/acs.jpcc.9b11369
J. Phys. Chem. C 2020, 124, 5452−5459

Authors

Pilar Carro − *Área de Química Física, Departamento de Química, Facultad de Ciencias, Instituto de Materiales y Nanotecnología, Universidad de La Laguna, La Laguna 38200, Tenerife, Spain;* orcid.org/0000-0001-8073-9857

Tim Albrecht − *Department of Chemistry, Imperial College London, London SW7 2AZ, U.K.;* orcid.org/0000-0001-6085-3206

Roberto C. Salvarezza − *Instituto de Investigaciones Fisicoquímicas Teóricas y Aplicadas (INIFTA), Facultad de Ciencias Exactas, Universidad Nacional de La Plata, CONICET, La Plata 1900, Argentina;* orcid.org/0000-0002-7617-4539

Complete contact information is available at: https://pubs.acs.org/10.1021/acs.jpcc.9b11369

Notes

The authors declare no competing financial interest.

■ ACKNOWLEDGMENTS

E.P. and T.A. would like to thank the Leverhulme Trust (RPG 2014-225). R.C.S. thanks the financial support from ANPCyT (PICT 2016-0679). P.C. thankfully acknowledges the computer resources provided by the Computer Support Service for Re-search (SAII) at La Laguna University (Spain) and the financial support from MINECO (ENE2016-74889-C4-2-R, AEI-FEDER-UE).

■ REFERENCES

(1) Jin, R.; Zeng, C.; Zhou, M.; Chen, Y. Atomically Precise Colloidal Metal Nanoclusters and Nanoparticles: Fundamentals and Opportunities. *Chem. Rev.* **2016**, *116*, 10346−10413.

(2) Kang, X.; Chong, H.; Zhu, M. Au25(SR)18: the captain of the great nanocluster ship. *Nanoscale* **2018**, *10*, 10758−10834.

(3) Qian, H.; Jin, R. Controlling Nanoparticles with Atomic Precision: The Case of Au144(SCH2CH2Ph)60. *Nano Lett.* **2009**, *9*, 4083−4087.

(4) Lopez-Acevedo, O.; Akola, J.; Whetten, R. L.; Grönbeck, H.; Häkkinen, H. Structure and Bonding in the Ubiquitous Icosahedral Metallic Gold Cluster Au144(SR)60. *J. Phys. Chem. C* **2009**, *113*, 5035−5038.

(5) Dainese, T.; Agrachev, M.; Antonello, S.; Badocco, D.; Black, D. M.; Fortunelli, A.; Gascón, J. A.; Stener, M.; Venzo, A.; Whetten, R. L.; et al. Atomically precise Au144(SR)60 nanoclusters (R = Et, Pr) are capped by 12 distinct ligand types of 5-fold equivalence and display gigantic diastereotopic effects. *Chem. Sci.* **2018**, *9*, 8796−8805.

(6) Zhu, M.; Aikens, C. M.; Hollander, F. J.; Schatz, G. C.; Jin, R. Correlating the Crystal Structure of A Thiol-Protected Au25Cluster and Optical Properties. *J. Am. Chem. Soc.* **2008**, *130*, 5883−5885.

(7) Heaven, M. W.; Dass, A.; White, P. S.; Holt, K. M.; Murray, R. W. Crystal Structure of the Gold Nanoparticle [N(C8H17)4][Au25-(SCH2CH2Ph)18]. *J. Am. Chem. Soc.* **2008**, *130*, 3754−3755.

(8) Akola, J.; Walter, M.; Whetten, R. L.; Häkkinen, H.; Grönbeck, H. On the Structure of Thiolate-Protected Au25. *J. Am. Chem. Soc.* **2008**, *130*, 3756−3757.

(9) Pensa, E.; Cortés, E.; Corthey, G.; Carro, P.; Vericat, C.; Fonticelli, M. H.; Benítez, G.; Rubert, A. A.; Salvarezza, R. C. The Chemistry of the Sulfur-Gold Interface: In Search of a Unified Model. *Acc. Chem. Res.* **2012**, *45*, 1183−1192.

(10) Häkkinen, H. The Gold-Sulfur Interface at the Nanoscale. *Nat. Chem.* **2012**, *4*, 443−455.

(11) Guo, Q.; Li, F. Self-Assembled Alkanethiol Monolayers on Gold Surfaces: Resolving the Complex Structure at the Interface by Stm. *Phys. Chem. Chem. Phys.* **2014**, *16*, 19074−19090.

(12) Maksymovych, P.; Voznyy, O.; Dougherty, D. B.; Sorescu, D. C.; Yates, J. T. Gold Adatom as a Key Structural Component in Self-Assembled Monolayers of Organosulfur Molecules on Au(111). *Prog. Surf. Sci.* **2010**, *85*, 206−240.

(13) Reimers, J. R.; Ford, M. J.; Halder, A.; Ulstrup, J.; Hush, N. S. Gold surfaces and nanoparticles are protected by Au(0)-thiyl species and are destroyed when Au(I)-thiolates form. *Proc. Natl. Acad. Sci. U.S.A.* **2016**, *113*, No. E1424.

(14) Pensa, E.; Albrecht, T. Controlling the Dynamic Instability of Capped Metal Nanoparticles on Metallic Surfaces. *J. Phys. Chem. Lett.* **2018**, *9*, 57−62.

(15) Cao, H.; Waghray, D.; Knoppe, S.; Dehaen, W.; Verbiest, T.; De Feyter, S. Tailoring Atomic Layer Growth at the Liquid-Metal Interface. *Nat. Commun.* **2018**, *9*, 4889.

(16) Hosseini, S.; Alsiraey, N.; Riley, A. J.; Zubkov, T.; Closson, T.; Tye, J.; Bodappa, N.; Li, Z. Variable Growth and Characterizations of Monolayer-Protected Gold Nanoparticles Based on Molar Ratio of Gold and Capping Ligands. *Langmuir* **2018**, *34*, 15517−15525.

(17) Zhang, B.; Sels, A.; Salassa, G.; Pollitt, S.; Truttmann, V.; Rameshan, C.; Llorca, J.; Olszewski, W.; Rupprechter, G.; Bürgi, T.; et al. Front Cover: Ligand Migration from Cluster to Support: A Crucial Factor for Catalysis by Thiolate-protected Gold Clusters (ChemCatChem 23/2018). *ChemCatChem* **2018**, *10*, 5337.

(18) Albrecht, T.; Mertens, S. F. L.; Ulstrup, J. Intrinsic Multistate Switching of Gold Clusters through Electrochemical Gating. *J. Am. Chem. Soc.* **2007**, *129*, 9162−9167.

(19) Kazan, R.; Müller, U.; Bürgi, T. Doping of Thiolate Protected Gold Clusters through Reaction with Metal Surfaces. *Nanoscale* **2019**, *11*, 2938−2945.

(20) Yao, Q.; Feng, Y.; Fung, V.; Yu, Y.; Jiang, D.-e.; Yang, J.; Xie, J. Precise Control of Alloying Sites of Bimetallic Nanoclusters Via Surface Motif Exchange Reaction. *Nat. Commun.* **2017**, *8*, 1555.

(21) Krishnadas, K. R.; Natarajan, G.; Baksi, A.; Ghosh, A.; Khatun, E.; Pradeep, T. Metal-Ligand Interface in the Chemical Reactions of Ligand-Protected Noble Metal Clusters. *Langmuir* **2019**, *35*, 11243−11254.

(22) Krishnadas, K. R.; Ghosh, A.; Baksi, A.; Chakraborty, I.; Natarajan, G.; Pradeep, T. Intercluster Reactions between Au25(SR)-18 and Ag44(SR)30. *J. Am. Chem. Soc.* **2016**, *138*, 140−148.

(23) Wang, S.; Abroshan, H.; Liu, C.; Luo, T.-Y.; Zhu, M.; Kim, H. J.; Rosi, N. L.; Jin, R. Shuttling Single Metal Atom into and out of a Metal Nanoparticle. *Nat. Commun.* **2017**, *8*, 848.

(24) Malola, S.; Nieminen, P.; Pihlajamäki, A.; Hämäläinen, J.; Kärkkäinen, T.; Häkkinen, H. A Method for Structure Prediction of Metal-Ligand Interfaces of Hybrid Nanoparticles. *Nat. Commun.* **2019**, *10*, 3973.

(25) Weng, B.; Lu, K.-Q.; Tang, Z.; Chen, H. M.; Xu, Y.-J. Stabilizing Ultrasmall Au Clusters for Enhanced Photoredox Catalysis. *Nat. Commun.* **2018**, *9*, 1543.

(26) Parker, J. F.; Weaver, J. E. F.; McCallum, F.; Fields-Zinna, C. A.; Murray, R. W. Synthesis of Monodisperse [Oct4N+][Au25(SR)-18−] Nanoparticles, with Some Mechanistic Observations. *Langmuir* **2010**, *26*, 13650−13654.

(27) Horcas, I.; Fernández, R.; Gómez-Rodríguez, J. M.; Colchero, J.; Gómez-Herrero, J.; Baro, A. M. WSxM: A Software for Scanning Probe Microscopy and a Tool for Nanotechnology. *Rev. Sci. Instrum.* **2007**, *78*, 013705.

(28) Kresse, G.; Joubert, D. From Ultrasoft Pseudopotentials to the Projector Augmented-Wave Method. *Phys. Rev. B: Condens. Matter Mater. Phys.* **1999**, *59*, 1758−1775.

(29) Kresse, G.; Hafner, J. Ab Initio Molecular Dynamics for Liquid Metals. *Phys. Rev. B: Condens. Matter Mater. Phys.* **1993**, *47*, 558−561.

(30) Kresse, G.; Furthmüller, J. Efficiency of Ab-Initio Total Energy Calculations for Metals and Semiconductors Using a Plane-Wave Basis Set. *Comput. Mater. Sci.* **1996**, *6*, 15−50.

(31) Kresse, G.; Furthmüller, J. Efficient Iterative Schemes for Ab Initio Total-Energy Calculations Using a Plane-Wave Basis Set. *Phys. Rev. B: Condens. Matter Mater. Phys.* **1996**, *54*, 11169−11186.

(32) Blöchl, P. E. Projector Augmented-Wave Method. *Phys. Rev. B: Condens. Matter Mater. Phys.* **1994**, *50*, 17953−17979.

(33) Grimme, S. Semiempirical GGA-Type Density Functional Constructed with a Long-Range Dispersion Correction. *J. Comput. Chem.* **2006**, *27*, 1787−1799.
(34) Grimme, S.; Antony, J.; Ehrlich, S.; Krieg, H. A Consistent and Accurate Ab Initio Parametrization of Density Functional Dispersion Correction (DFT-D) for the 94 Elements H-Pu. *J. Chem. Phys.* **2010**, *132*, 154104.
(35) Pearson, W. B. *A Handbook of Lattice Spacings and Structures of Metals and Alloys*; Pergamon Press, 1958.
(36) Monkhorst, H. J.; Pack, J. D. Special Points for Brillouin-Zone Integrations. *Phys. Rev. B: Condens. Matter Mater. Phys.* **1976**, *13*, 5188−5192.
(37) Carro, P.; Torrelles, X.; Salvarezza, R. C. A Novel Model for the $(\sqrt{3}\times\sqrt{3})$R30° Alkanethiolate−Au(111) Phase Based on Alkanethiolate−Au Adatom Complexes. *Phys. Chem. Chem. Phys.* **2014**, *16*, 19017−19023.
(38) Carro, P.; Pensa, E.; Vericat, C.; Salvarezza, R. C. Hydrocarbon Chain Length Induces Surface Structure Transitions in Alkanethiolate−Gold Adatom Self-Assembled Monolayers on Au(111). *J. Phys. Chem. C* **2013**, *117*, 2160−2165.
(39) Carro, P.; Salvarezza, R. C. Gold Adatoms Modulate Sulfur Adsorption on Gold. *Nanoscale* **2019**, *11*, 19341−19351.
(40) Taylor, M. G.; Mpourmpakis, G. Thermodynamic Stability of Ligand-Protected Metal Nanoclusters. *Nat. Commun.* **2017**, *8*, 15988.
(41) Packwood, D. M.; Han, P.; Hitosugi, T. Chemical and Entropic Control on the Molecular Self-Assembly Process. *Nat. Commun.* **2017**, *8*, 14463.
(42) Bürgi, T. Properties of the Gold−Sulphur Interface: From Self-Assembled Monolayers to Clusters. *Nanoscale* **2015**, *7*, 15553−15567.
(43) Arce, F. T.; Vela, M. E.; Salvarezza, R. C.; Arvia, A. J. Dynamic Characteristics of Adsorbed Monolayers of 1-Dodecanethiol on Gold (111) Terraces from in-Situ Scanning Tunneling Microscopy Imaging. *Electrochim. Acta* **1998**, *44*, 1053−1067.
(44) Yu, M.; Bovet, N.; Satterley, C. J.; Bengió, S.; Lovelock, K. R. J.; Milligan, P. K.; Jones, R. G.; Woodruff, D. P.; Dhanak, V. True Nature of an Archetypal Self-Assembly System: Mobile Au-Thiolate Species on Au(111). *Phys. Rev. Lett.* **2006**, *97*, 166102.
(45) Holmes, S.; Gao, J.; Tang, L.; Li, F.; Palmer, R. E.; Guo, Q. Bridge-Bonded Methylthiolate on Au(111) Observed with the Scanning Tunneling Microscope. *Phys. Chem. Chem. Phys.* **2018**, *20*, 19486−19491.
(46) Holmes, S.; Palmer, R. E.; Guo, Q. The Diffusion of $Au(CH_3S)_2$ on Au(111) Observed with the Scanning Tunneling Microscope. *J. Phys. Chem. C* **2019**, *123*, 24104−24110.
(47) Wang, G.; Rühling, A.; Amirjalayer, S.; Knor, M.; Ernst, J. B.; Richter, C.; Gao, H.-J.; Timmer, A.; Gao, H.-Y.; Doltsinis, N. L.; et al. Ballbot-Type Motion of N-Heterocyclic Carbenes on Gold Surfaces. *Nat. Chem.* **2016**, *9*, 152.
(48) Walen, H.; Liu, D.-J.; Oh, J.; Lim, H.; Evans, J. W.; Aikens, C. M.; Kim, Y.; Thiel, P. A. Cu_2S_3 Complex on Cu(111) as a Candidate for Mass Transport Enhancement. *Phys. Rev. B: Condens. Matter Mater. Phys.* **2015**, *91*, 045426.
(49) González, M. C. R.; Carro, P.; Pensa, E.; Vericat, C.; Salvarezza, R.; Hernández Creus, A. The Role of a Double Molecular Anchor on the Mobility and Self-Assembly of Thiols on Au(111): The Case of Mercaptobenzoic Acid. *ChemPhysChem* **2017**, *18*, 804−811.
(50) Rosei, F.; Schunack, M.; Naitoh, Y.; Jiang, P.; Gourdon, A.; Laegsgaard, E.; Stensgaard, I.; Joachim, C.; Besenbacher, F. Properties of Large Organic Molecules on Metal Surfaces. *Prog. Surf. Sci.* **2003**, *71*, 95−146.
(51) Castez, M. F.; dos Santos Claro, P. C.; Schilardi, P. L.; Andreasen, G.; Salvarezza, R. C. Surface Relaxation of High-Aspect-Ratio Nanostructures: Theory and Experiments. *J. Phys. Chem. C* **2010**, *114*, 4603−4610.
(52) Madrid, M. A.; Salvarezza, R. C.; Castez, M. F. Surface-Diffusion-Driven Decay of High-Aspect-Ratio Gratings: Existence of Morphologically Related Classes. *Phys. Rev. E: Stat., Nonlinear, Soft Matter Phys.* **2013**, *87*, 062407.
(53) Baksi, A.; Chakraborty, P.; Bhat, S.; Natarajan, G.; Pradeep, T. $[Au_{25}(SR)_{18}]_2^{2-}$: A Noble Metal Cluster Dimer in the Gas Phase. *Chem. Commun.* **2016**, *52*, 8397−8400.
(54) Li, F.-S.; Zhou, W.; Guo, Q. Uncovering the Hidden Gold Atoms in a Self-Assembled Monolayer of Alkanethiol Molecules on Au(111). *Phys. Rev. B: Condens. Matter Mater. Phys.* **2009**, *79*, 113412.

https://dx.doi.org/10.1021/acs.jpcc.9b11369
J. Phys. Chem. C 2020, 124, 5452−5459